water

MDPI

Article

Preparation of Magnetic Surface Ion-Imprinted Polymer Based on Functionalized Fe_3O_4 for Fast and Selective Adsorption of Cobalt Ions from Water

Zijian Zhao [1,†], Hui Jiang [1,†], Lang Wu [1], Ning Yu [1], Zhengwei Luo [2] and Wenhua Geng [1,*]

[1] College of Biotechnology and Pharmaceutical Engineering, Nanjing Tech University, 30# Puzhu South Road, Nanjing 211816, China; zhaozijian@njtech.edu.cn (Z.Z.); huijiang@njtech.edu.cn (H.J.); wulang1994as@163.com (L.W.); 202061218188@njtech.edu.cn (N.Y.)

[2] School of Environmental Science and Engineering, Nanjing Tech University, 30# Puzhu South Road, Nanjing 211816, China; luozw1989@163.com

* Correspondence: gengwenhua@njtech.edu.cn

† These authors contributed equally to this work.

Abstract: A novel cobalt ion-imprinted polymer (Co(II)-MIIP) based on magnetic Fe_3O_4 nanoparticles was prepared by using Co(II) as the template ion, and bis(2-methacryloxyethyl) phosphate and glycylglycine as dual functional monomers. The fabricated material was analyzed by Fourier transform infrared spectroscopy, thermogravimetric analysis, field emission scanning electron microscopy, energy dispersive X-ray spectroscopy, Brunauer–Emmett–Teller, X-ray diffraction, and vibrating sample magnetometer. The adsorption experiments with Co(II)-MIIP, found that the maximum adsorption capacity could reach 33.4 $mg \cdot g^{-1}$, while that of the non-imprinted polymer (Co(II)-NIP) was found to reach 15.7 $mg \cdot g^{-1}$. The adsorption equilibriums of Co(II)-MIIP and Co(II)-NIP was established within 20 min and 30 min, respectively. The adsorption process could be suitably described by the Langmuir isotherm model and the pseudo-second-order kinetics model. In binary mixtures of Co(II)/Fe(II), Co(II)/Cu(II), Co(II)/Mg(II), Co(II)/Zn(II), and Co(II)/Ni(II), the relative selectivity coefficients of Co(II)-MIIP toward Co(II)-NIP were 5.25, 4.05, 6.06, 11.81, and 4.48, respectively. The regeneration experiments indicated that through six adsorption–desorption cycles, the adsorption capacity of Co(II)-MIIP remained nearly 90%.

Keywords: cobalt; ion-imprinted polymers; magnetic nanoparticles; dual monomers; selective adsorption

Citation: Zhao, Z.; Jiang, H.; Wu, L.; Yu, N.; Luo, Z.; Geng, W. Preparation of Magnetic Surface Ion-Imprinted Polymer Based on Functionalized Fe_3O_4 for Fast and Selective Adsorption of Cobalt Ions from Water. *Water* **2022**, *14*, 261. https://doi.org/10.3390/w14020261

Academic Editor: Laura Bulgariu

Received: 7 December 2021
Accepted: 13 January 2022
Published: 17 January 2022

1. Introduction

Cobalt (Co) has excellent hardness, thermal fatigue resistance, and magnetic property, leading to the wide use of Co and Co compounds in various industrial fields, such as mining, metallurgy, electroplating, paint, and electronics [1]. As a result, the discharge of Co contained wastewater from industrial activities causes severe environmental pollution, as well as health threats to human beings [2,3]. The Co content in an adult's body is generally about 1.1 mg. A small amount of Co can cause anemia, while an excessive amount of Co can cause poisoning [4].

Until now, the treatment of wastewater containing Co has raised substantial concern, and researchers continue to explore ways to efficiently remove Co in industrial wastewater, such as biological treatment [5], chemical precipitation [6], electrochemical methods [7], membrane separation [8], and adsorption. Among these methods, adsorption is thought to be an economical and effective method for removing Co(II) ions from aqueous solutions among used methods. Vivas et al. [9] investigated the performance of dicalcium phosphate dihydrate as an adsorbent in treating Co waste liquid, but the recycling efficiency was found to be low. Tawfik et al. [10] synthesized a new hydrophobic cross-linked polyzwitterionic acid, which displayed a superior capability to adsorb Co(II) ions and assisted with

the adsorption of organic pollutants. Mostafa et al. [11] prepared a magnetic chitosan using 8-hydroxyquinoline to remove Co(II) ions from aqueous solutions. Regretfully, these adsorbents have several shortcomings in practical applications, such as insufficient recycling performance, poor selectivity, and long acting time. Thus, synthesizing new adsorbents for quick and selective removal of Co from wastewater is urgently needed.

Ion-imprinted polymers (IIPs) are designed based on molecularly imprinted technique [12]. Metal ions can be imprinted as template ions for complexation to polymerizable ligands [13]. After removing the template ions, the resulting polymers can possess a strong affinity to template ions, and the polymer memory effect of IIPs enables specific ligands to selectively recognize target ions. So far, various metal ion-imprinted polymers have been reported. Angkana et al. [14] used the suspension polymerization to prepare copper-imprinted polymers. Huang et al. [15] studied Cr(VI) ion-imprinted polymer on graphene oxide-mesoporous silica nanosheets. Zhang et al. [16] synthesized Mo(VI)-imprinted chitosan/triethanolamine gel beads by using ion-imprinted technology. Lee et al. [17] synthesized a magnetic Co(II)-imprinted polymer based on mesoporous silica for the selective removal of Co(II) ions. To realize the fast adsorption of target ions, surface ion imprinted polymers were prepared using silica, chitosan, and Fe_3O_4, etc., as carriers to support the ion imprinted layer. In comparison, Fe_3O_4 nanoparticles (NPs) have shown superior properties to other carriers, such as stable physical properties, higher surface area, and excellent magnetic properties, which can be used as an ideal carrier for IIPs.

In this study, a novel Co(II)-imprinted polymer was prepared using magnetic Fe_3O_4 NPs modified with tetraethyl orthosilicate and methacryloxy propyl trimethoxyl silane as the support. The easy separability was one of the advantages of magnetic materials for waste water treatment, and the magnetic materials had a unique role of rapid separation and recovering by applying an external magnetic field [18]. Bis(2-methacryloxyethyl) phosphate (B-2MP) and glycylglycine (GG) were used as dual monomers. The joint action of dual monomers endows the resultant ion imprinted adsorbents with higher selectivity and adsorption rate towards target ions, due to the strong affinity between multiple functional groups and target ions [19]. The final product was characterized, and the adsorption properties were investigated as well.

2. Materials and Methods

2.1. Materials

Ferrous chloride tetrahydrate ($FeCl_2{\cdot}4H_2O$) and ferric chloride hexahydrate ($FeCl_3{\cdot}6H_2O$) were purchased from Sinopharm Chemical Reagent Co., Ltd. (Shanghai, China). Bis(2-methacryloxyethyl) phosphate (B-2MP), glycylglycine (GG), ethylene glycol methacrylate (EGDMA), *N*,*N*-azobisisobutyronitrile (AIBN), tetraethyl orthosilicate (TEOS), and γ-methacryloxy propyl trimethoxyl silane (MPS) were purchased from Aladdin Industrial Corporation (Shanghai, China). Cobaltous nitrate hexahydrate ($Co(NO_3)_2{\cdot}6H_2O$) was purchased from Nanjing Chemical Reagent Co., Ltd. (Nanjing, China). All chemical reagents employed in this work were of reagent grade.

2.2. Synthesis of Fe_3O_4 NPs

Uniform Fe_3O_4 magnetic NPs were synthesized by a chemical co-precipitation method based on our previous work [20]. First, 2.12 g of $FeCl_2{\cdot}4H_2O$ and 4.86 g of $FeCl_3{\cdot}6H_2O$ were dissolved in 110 mL of deionized water saturated with nitrogen gas (N_2), then the mixture was heated up to 80 °C under N_2 atmosphere in a four-necked flask. After 10 mL of ammonia aqueous solution (25%, *w*/*w*) was added dropwise under vigorous mechanical stirring, the brown solution gradually turned black. The mixed solution was stirred vigorously for 30 min under N_2 atmosphere until black Fe_3O_4 NPs were obtained. The synthesized Fe_3O_4 NPs were rinsed with deionized water and dried in vacuum at 45 °C for 8 h.

2.3. Surface Silanization of Fe_3O_4 NPs

Fe_3O_4 NPs (1.0 g) were dispersed in 120 mL of absolute ethanol, then 20 mL of deionized water and ammonia aqueous solution (25%, *w*/*w*) were added [21]. Hereafter, 2 mL of TEOS was added dropwise to the mixed solution and kept stirring for 12 h at room temperature. After the reaction, the silanized Fe_3O_4 NPs (Fe_3O_4@SiO_2) were separated under an external magnet, rinsed with deionized water, and dried in vacuum at 40 °C for 8 h.

2.4. Functionalization of Fe_3O_4@SiO_2

The prepared Fe_3O_4@SiO_2 NPs (0.5 g) were dispersed into 80 mL of ethanol aqueous solution (15%, *v*/*v*) under sonication to form a suspension. Next, 2 mL of MPS was added dropwise under mechanical stirring [22]. The reaction lasted 12 h at 40 °C. After the reaction, the functionalized Fe_3O_4@SiO_2 (Fe_3O_4@SiO_2@MPS) were rinsed with absolute ethanol and deionized water. Finally, the product was dried in vacuum at 60 °C for 8 h.

2.5. Synthesis of Co(II)-MIIP and Co(II)-NIP

Fe_3O_4@SiO_2@MPS (0.5 g) was dispersed uniformly into 60 mL of ethanol aqueous solution (60%, *v*/*v*) by sonication for 20 min to form a suspension (a). At the same time, B-2MP and GG with different ratios (i.e., 0:0, 5:0, 4:1, 3:2, 1:1, 2:3, 1:4, 0:5) were added to 60 mL of ethanol aqueous solution (60%, *v*/*v*) which dissolved 2 mmol of $Co(NO_3)_2{\cdot}6H_2O$ to form a solution (b). Solution (b) was stirred for 120 min to reach the fully complexing of Co(II) with B-2MP and GG. The suspension (c) was obtained by mixing the suspension (a) with the solution (b) under mechanical stirring. Afterward, EGDMA with different amounts (2–20 mmol) and 80 mg of AIBN were added to the suspension (c). The magnetic cobalt ion-imprinted polymer (Co(II)-MIIP) containing Co(II) ions was obtained after polymerization under N_2 atmosphere at 60 °C for 24 h.

Later, the Co(II)-MIIP containing template ions were rinsed with ethanol and deionized water. Co(II) ions were eluted from ion-imprinted polymers with 0.05 $mol{\cdot}L^{-1}$ NaOH for 120 min until Co(II) ions were not discovered in the elution solution. After the elution, the Co(II)-MIIP was rinsed repeatedly with deionized water, and the washed imprinting material was dried in vacuum at 60 °C for 12 h. By contrast, the same synthesis method was used to obtain magnetic non-imprinted polymers (MNIP), except that Co(II) ions were not added in the synthesis process. The preparation process of Co(II)-MIIP is shown in Figure 1.

2.6. Characterizations

The functional groups of prepared materials were analyzed by Fourier transform infrared spectroscopy (FT-IR, Nicolet 6700, Thermo Fisher, MA, USA). Scanning electron microscopy (SEM, Thermo Fisher, MA, USA), and energy dispersive spectroscopy (EDS) were used to analyze the surface morphology of the materials and the types of elements. Thermogravimetric analysis (TGA) was used to analyze the thermal stability (Perkin Elmer TGA 400, New Castle, DE, USA). The Brunauer–Emmett–Teller (BET) equation was used to determine the surface area and pore sizes (V-Sorb 2800 Series Analyzer, Gold APP Instrument, Beijing, China). The vibrating sample magnetometer (VSM, VersaLab, CA, USA) was used to analyze the magnetic property. XRD patterns were determined by using the X-ray diffractometer (XRD, SmartLab, TKY, Japan) from 10° to 90°.

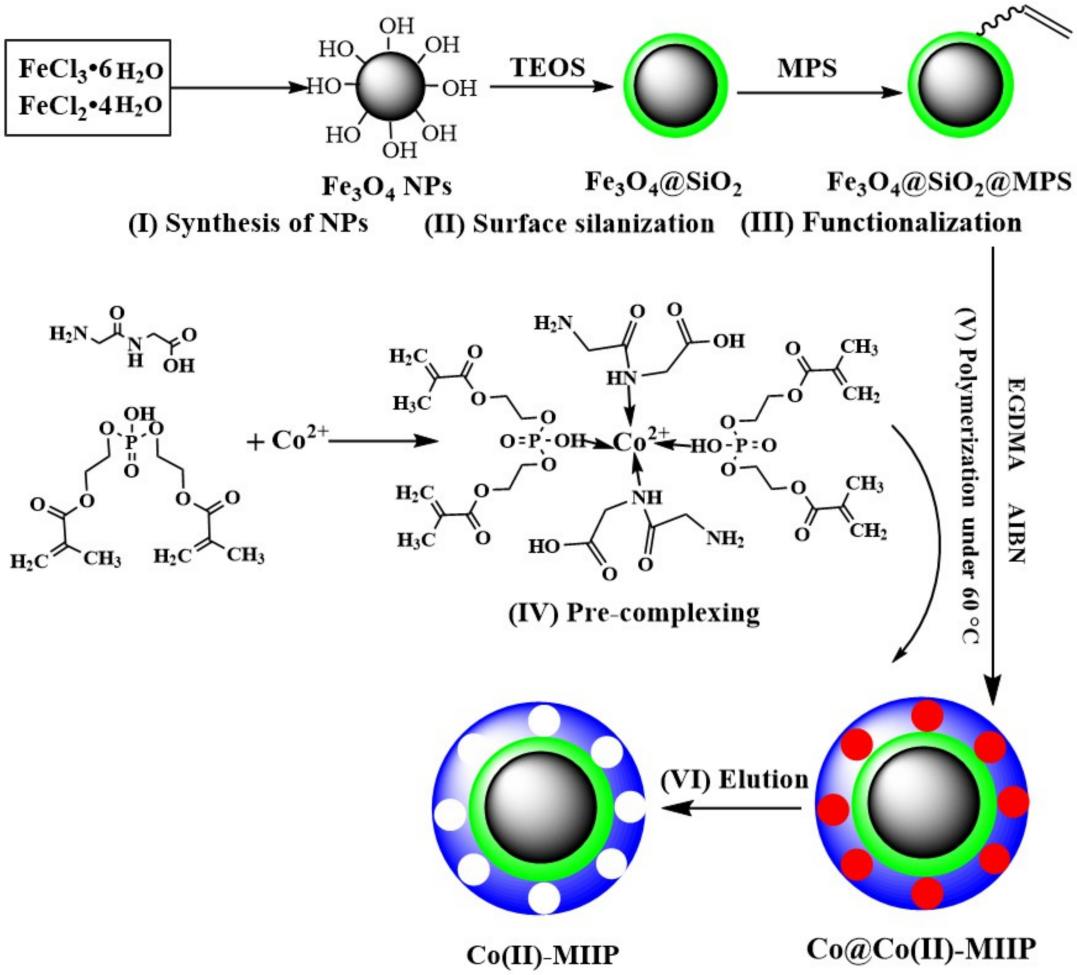

Figure 1. The schematic diagram for the synthesis of Co(II)-MIIP.

2.7. Adsorption Experiments

The simulated Co(II) ions solution was used in the adsorption experiment. The prepared adsorbents (10 mg) were added into 10 mL of Co(II) ions solution, which was then shaken at 25 °C. Over a certain period, the adsorbent was separated and recovered by the magnet, and the solution was filtered with the filter head (0.45 μm). Then, the residual Co(II) ions were determined by inductively coupled plasma-optical emission spectrometer (ICP-OES, iCAP 6300, Thermo Fisher, USA). The adsorption capacity q_e (mg·g^{-1}) could be computed using Equation (1):

$$qe = \frac{(ci - ce)V}{m} \quad (1)$$

where c_i (mg·L^{-1}) is the initial concentrations of Co(II) ions, and c_e (mg·L^{-1}) is the equilibrium concentrations; V (L) is the volume of the liquid; m (g) is the mass of adsorbents.

The influence of solution pH on the adsorption capacity of adsorbents were investigated by using simulated Co(II) ions solution with pH values ranging from 3.0 to 8.5. The adsorption capacity of the adsorbents was calculated based on the variations of Co(II) concentration at intervals, and the resultant adsorption curves were fitted by using pseudo-first-order and pseudo-second-order models, respectively. The equilibrium adsorption isotherms were carried out with the original concentration ranges from 20–500 mg·L^{-1}, and Langmuir isotherm equation and Freundlich isotherm equation were used to fit the equilibrium adsorption experimental data, respectively.

2.8. Adsorption Selectivity

To research the adsorption selectivity, Cu(II), Zn(II), Ni(II), Mg(II), and Fe(II) were also added into the solution of Co(II) ions. Each concentration was 100 mg·L^{-1} in binary mixtures. In 10 mL of different dual-system solutions, the amount of adsorbent (Co(II)-MIIP or Co(II)-NIP) was 1.0 g·L^{-1}. After the adsorption experiment, all concentration of Co(II) ions and competing ions were determined by ICP-OES. The distribution coefficient (K_d, L·g^{-1}) and selectivity coefficient (K) were calculated by using Equations (2) and (3) [23]. The relative selectivity coefficient (K') was calculated using Equation (4) [24]:

$$Kd = \frac{q_e}{C_e} \tag{2}$$

$$K = \frac{K_d\ (template\ ion)}{K_d\ (Competing\ ions)} \tag{3}$$

$$K' = \frac{K_{IIP}}{K_{NIP}} \tag{4}$$

3. Results and Discussion

3.1. B-2MP and GG Dosage

The effect of the addition amount of B-2MP and GG on the adsorption performance is shown in Figure 2. When monomers were not added in the synthesis process, the adsorption capacity of Co(II)-MIIP was only 2.3 mg·g^{-1}. When only B-2MP or GG was added in the synthesis process, that of Co(II)-MIIP was 18.1 mg·g^{-1} and 10.3 mg·g^{-1}, respectively; this was due to the Schiff base nitrogen and carboxyl oxygen having good complexing ability [25]. It showed that the monomer had a significant effect on the adsorption performance, and the complexation between B-2MP and template ion was stronger than that of GG. The highest adsorption capacity was obtained when B-2MP: GG was 4:1, indicating that the presence of GG could enhance the complexation between B-2MP and the template ion. This may be due to more chelates. Therefore, the best ratio of monomer B-2MP and GG was 4:1.

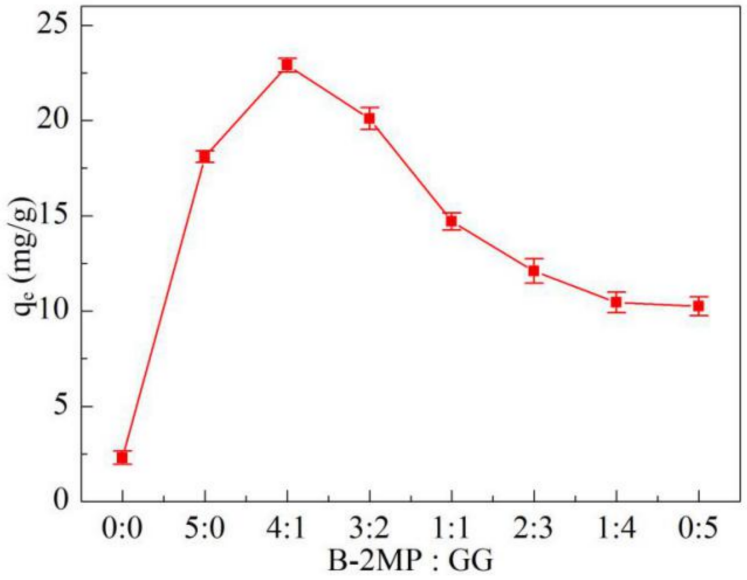

Figure 2. Effect of different ratios between B-2MP and GG on the adsorption capacity of Co(II)-MIIP.

3.2. The Amount of EGDMA

The effect of EGDMA usage on the adsorption performance is illustrated in Figure 3. When the addition amount of EGDMA was in a range of 2–12 mmol, the adsorption capacity of Co(II)-MIIP increased rapidly as the increase of the addition amount of EGDMA. The monomer-ion prepolymerized unit was fully cross-linked due to sufficient EGDMA,

resulting in abundant specific imprinting sites on the surface of the imprinting material. However, when EGDMA was over-dosed, there was a decrease in the saturated adsorption capacity. The cross-linking agent made an important impact to the preparation process of IIPs. The excessive cross-linking agent would self-polymerize on the surface of the adsorbent, which not only caused the specific surface area of the imprinted material decrease, but also made it difficult to elute the template ions [26]. Therefore, the optimal addition amount of the crosslinking agent EGDMA was 12 mmol.

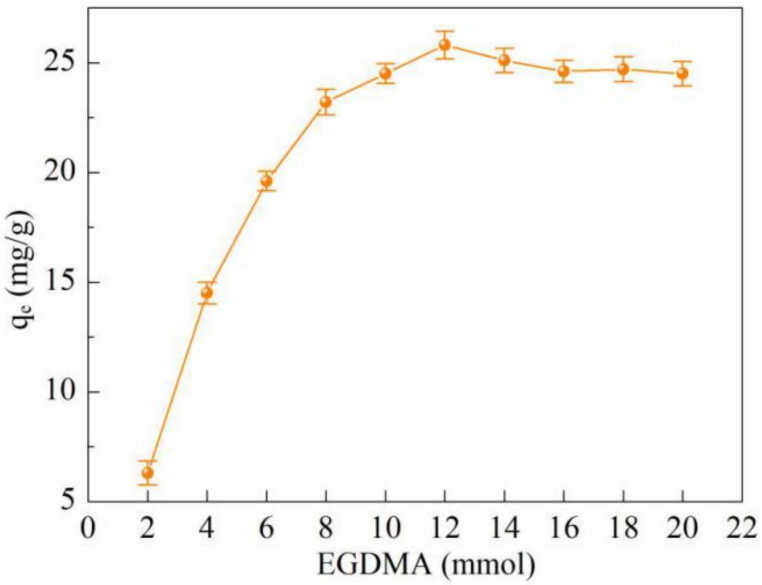

Figure 3. Effect of EGDMA amount on the adsorption capacity of Co(II)-MIIP.

3.3. FT-IR

The absorption peaks of Fe_3O_4 NPs, Fe_3O_4@SiO_2, Fe_3O_4@SiO_2@MPS, and Co(II)-MIIP were analyzed by FT-IR in the wavenumber range of 500–4000 cm^{-1}, as shown in Figure 4. In curve (a), the peak at 596 cm^{-1} was due to the asymmetric vibration of Fe-O, and the peak at 3438.5 cm^{-1} was due to the hydroxyl groups of Fe_3O_4 NPs or the residual water in the sample [3,27]. The existence of these characteristic peaks proves the successful preparation of Fe_3O_4 NPs [28]. In curve (b), the peaks at 796 cm^{-1} and 942 cm^{-1} were attributed to Si-O stretching vibration, and the stretching vibration of Si-O-Si caused the peak at 1013 cm^{-1}. The absorption peak indicated that Fe_3O_4 NPs were successfully modified by TEOS [29]. In curve (c), the peak located at 1434 cm^{-1} was the characteristic peak of C=C, and the peak at 1621 cm^{-1} was ascribed to the C=O bond. The peaks at 2951 cm^{-1} and 3055 cm^{-1} were the characteristic peaks of -CH_2 and -CH_3, respectively. These absorption peaks were all derived from the silane coupling agent MPS [30]. In curve (d), the N-H tensile vibration from the monomer GG caused the absorption peak at 764 cm^{-1}, and the C=N stretching vibration caused the peak located at 1728 cm^{-1}. Moreover, the -NH_2 asymmetric vibration caused the absorption peak at 3421 cm^{-1} [25]. Furthermore, the absorption peaks at 1158 cm^{-1} and 1260 cm^{-1} were attributed to the P=O of monomer B-2MP [31]. The existence of the above characteristic peaks proved the successful preparation of Co(II)-MIIP.

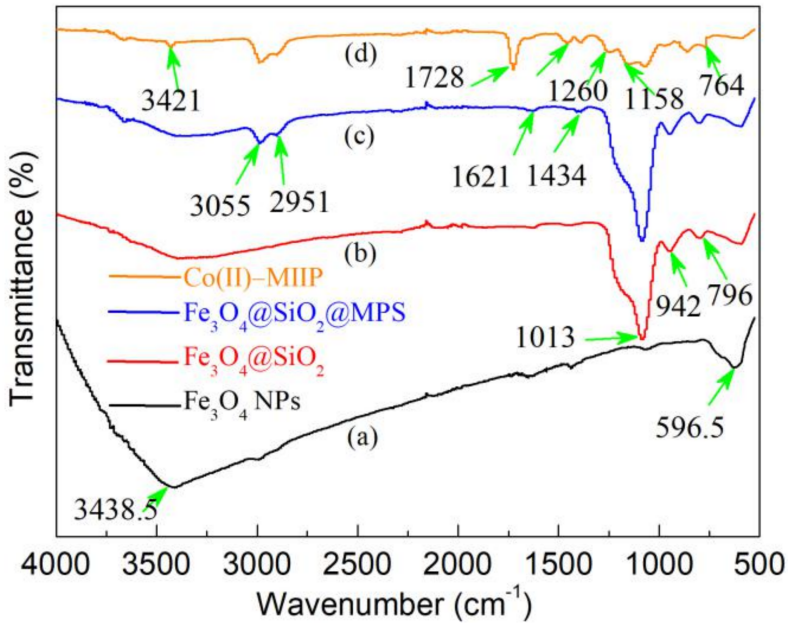

Figure 4. FT-IR spectra of (**a**) Fe_3O_4 NPs, (**b**) Fe_3O_4@SiO_2, (**c**) Fe_3O_4@SiO_2@MPS, and (**d**) Co(II)-MIIP.

3.4. TGA

The thermal stability of Fe_3O_4 NPs, Fe_3O_4@SiO_2@MPS, and Co(II)-MIIP was judged by the thermogravimetric analyzer, and the outcomes are shown in Figure 5. Fe_3O_4 NPs had no obvious weight loss in the temperature range of 30–600 °C, indicating that it had good thermal stability. The evaporation of residual water on the surface of Fe_3O_4 NPs caused a slight decrease in mass fraction, and the final mass fraction was 99.3%. The TGA curves of Fe_3O_4@SiO_2@MPS and Fe_3O_4 NPs within the temperature range of 30–600 °C have similar trends, but the high temperature decomposition of silane coupling agent on the surface caused the slope of the curve to be steeper, indicating that the quality was reduced more seriously. The final weight fraction was 93.6%. The weight loss of Co(II)-MIIP mainly went through three stages. The first stage arose in the range of 30–200 °C. The evaporation of moisture and residual reagents in the adsorbent was the main cause of weight loss in this stage. The second stage arose in 200–550 °C. The mass fraction of Co(II)-MIIP dropped sharply in the range of 200–350 °C because the organic imprinted layer (including EGDMA and monomers) loaded on the surface of Fe_3O_4 NPs, decomposed and volatilized rapidly at high temperature. From 350 to 550 °C, the further increase of temperature would cause the decomposition of some organic components with strong thermal stability. The remaining monomers and crosslinkers gradually volatilized. At this time, SiO_2 and MPS were also decomposed, resulting in the slow decrease in mass fraction. Finally, from 550 to 600 °C, the mass fraction of Co(II)-MIIP remained constant, indicating that the organic imprinted layer on the surface of Co(II)-MIIP had been completely decomposed. The remaining mass fraction of Fe_3O_4 NPs was 33.2%.

3.5. SEM and EDS

The surface morphology and microstructure of Fe_3O_4@SiO_2@MPS and CO(II)-MIIP were analyzed by SEM. The specific analysis are exhibited in Figure 6. The SEM image of Fe_3O_4@SiO_2@MPS (Figure 6a) shows that the particles were spherical with uniform particle size. According to the SEM image of Co(II)-MIIP (Figure 6b), the organic imprinted layer caused the surface of Co(II)-MIIP to be porous and rough. Furthermore, the Co(II)-MIIP particles were interconnected owing to agglomeration. Figure 6c,d shows the EDS characterization diagrams of Fe_3O_4@SiO_2@MPS and Co(II)-MIIP, respectively. Figure 6c mainly contains elements such as C, O, Fe, and Si. The presence of Fe indicated that the preparation of Fe_3O_4 NPs was successful, while the presence of Si and C was attributed

to the modification and functionalization process of Fe_3O_4 NPs. Compared with the EDS of Fe_3O_4@SiO_2@MPS, the N and P elements are shown in the diagram of Co(II)-MIIP, indicating that GG and B-2MP were involved in the polymerization process. The above elements proved that the polymer was successfully prepared.

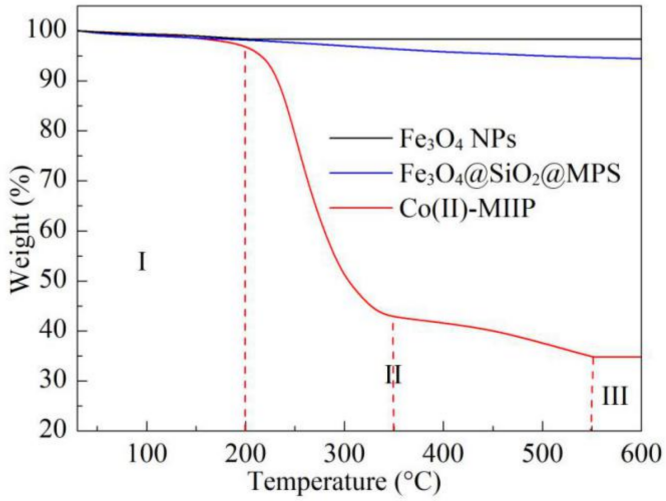

Figure 5. The weight loss curves of Fe_3O_4 NPs, Fe_3O_4@SiO_2@MPS, and Co(II)-MIIP.

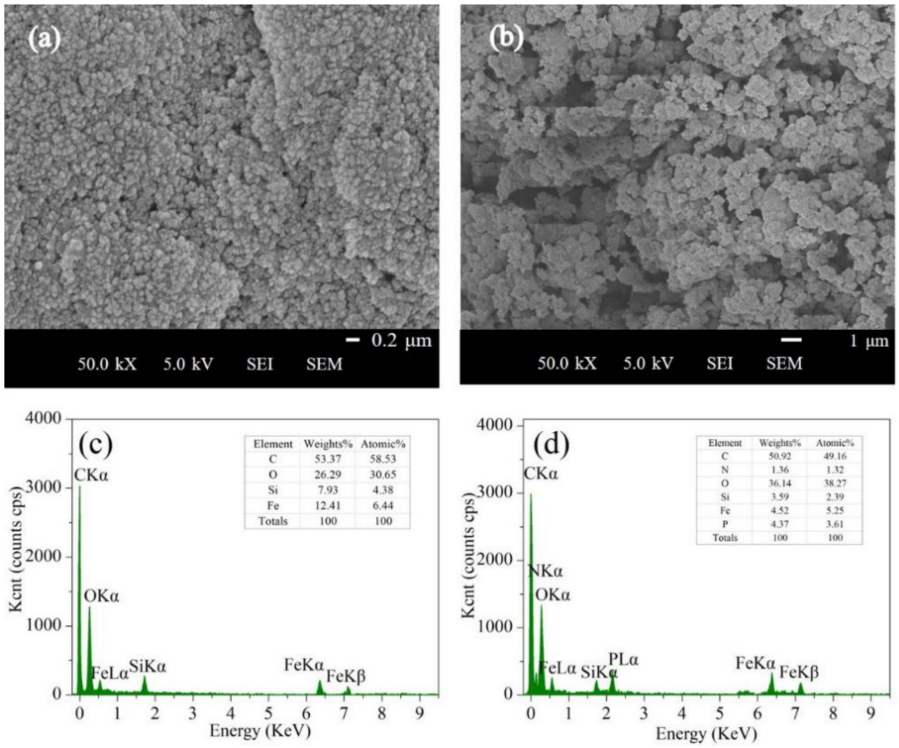

Figure 6. SEM micrographs of (**a**) Fe_3O_4@SiO_2@MPS and (**b**) Co(II)-MIIP, and EDS spectra of (**c**) Fe_3O_4@SiO_2@MPS and (**d**) Co(II)-MIIP.

3.6. BET

The N_2 adsorption–desorption isotherms and pore size distribution curves of Fe_3O_4@SiO_2@MPS and Co(II)-MIIP are exhibited in Figure 7. The N_2 adsorption capacity of Fe_3O_4@SiO_2@MPS and Co(II)-MIIP increased slowly in the low pressure region ($P/P_0 < 0.5$), and sharply increased in the high pressure region ($0.8 < P/P_0 < 1.0$), indicating that the N_2 isotherm of two materials belonged to category IV isotherm. There

were abundant mesoporous structures on the surface of the materials [32]. In addition, it could be found from the figure that the N_2 adsorption capacity of Fe_3O_4@SiO_2@MPS was significantly greater than that of Co(II)-MIIP. The Barrett–Joyner–Halenda method was used to determine the pore size, pore volume, and specific surface area of Fe_3O_4@SiO_2@MPS and Co(II)-MIIP [33]. The relevant results were shown in Table 1. The pore volume decreased from 0.4028 $cm^3 \cdot g^{-1}$ for Fe_3O_4@SiO_2@MPS to 0.2375 $cm^3 \cdot g^{-1}$ for Co(II)-MIIP, and the specific surface area also decreased from 126.82 $m^2 \cdot g^{-1}$ to 74.94 $m^2 \cdot g^{-1}$, which was attributed to the formed organic imprinting area [34]. However, the average pore diameter of Co(II)-MIIP (9.31 nm) was still in the mesoporous range (2 nm < d < 50 nm), indicating that it was a mesoporous material and suitable for ion adsorption [35]. Its pore structure increased the surface area and provided more adsorption sites. The rough and easily modifiable surface of nanoparticles was conducive to capturing Co(II) ions [36].

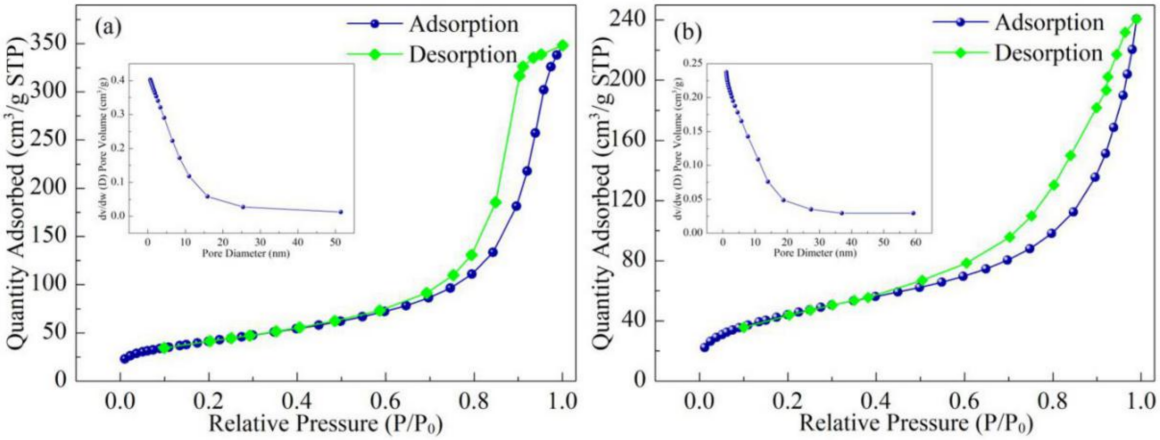

Figure 7. N_2 adsorption-desorption isotherms of (**a**) Fe_3O_4@SiO_2@MPS and (**b**) Co(II)-MIIP.

Table 1. The BET surface areas and pore parameters for Fe_3O_4@SiO_2@MPS and Co(II)-MIIP.

Samples	Average Pore Diameter (nm)	Total Pore Volume ($cm^3 \cdot g^{-1}$)	Specific Surface Area ($m^2 \cdot g^{-1}$)
Fe_3O_4@SiO_2@MPS	10.37	0.4028	126.82
Co(II)-MIIP	9.31	0.2375	74.94

3.7. VSM

The magnetic properties of Fe_3O_4@SiO_2@MPS and Co(II)-MIIP are illustrated in Figure 8. The hysteresis loops indicated that Fe_3O_4@SiO_2@MPS and Co(II)-MIIP were both superparamagnetic [37]. In addition, the results showed that the magnetic saturation intensity of Fe_3O_4@SiO_2@MPS was 36.1 emu/g, while that of Co(II)-MIIP was only 9.5 emu/g. Since the imprinted polymer layer loaded on the surface, the magnetic saturation intensity of Co(II)-MIIP was weakened. However, it is shown that Co(II)-MIIP in the solution could still be separated quickly under the action of an external magnetic field from the insert images in Figure 8.

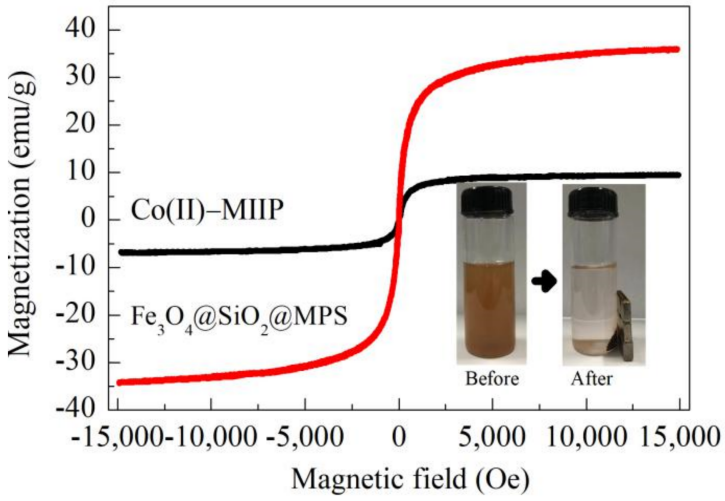

Figure 8. The VSM spectra of Fe_3O_4@SiO_2@MPS and Co(II)-MIIP, and the actual adsorption and separation procedure of Co(II)-MIIP.

3.8. XRD

The XRD patterns of Fe_3O_4, Fe_3O_4@SiO_2@MPS and Co(II)-MIIP were shown in Figure 9. For Fe_3O_4 NPs, the diffraction peaks matched well with that reported in the JCPDS-International Centre, which proved that the prepared Fe_3O_4 NPs had a good crystal structure [20]. After surface silanization, Fe_3O_4@SiO_2@MPS showed no significant difference with Fe_3O_4 NPs regarding both diffraction peaks and peak intensities. The characteristic diffraction peaks of Co(II)-MIIP were nearly unchanged, but the peak intensities obviously decreased. This can be explained by Fe_3O_4 NPs being encapsulated in Co(II)-MIIP, and the functional ion imprinted layer resulted in the attenuation of diffraction peaks [38]. However, the crystal structure of nanoparticles remained intact after surface functionalization [20].

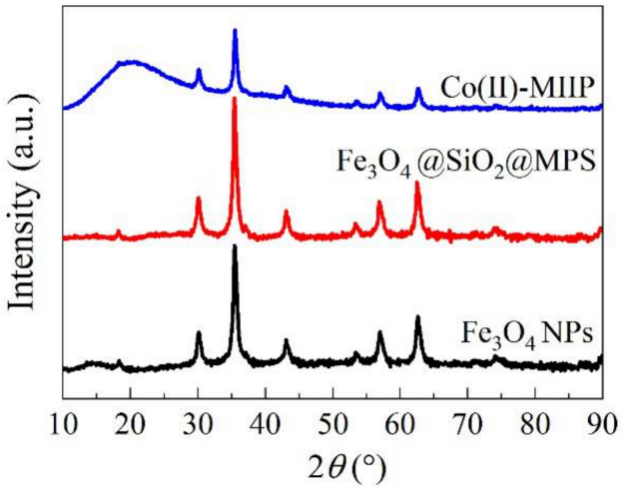

Figure 9. XRD patterns of Fe_3O_4, Fe_3O_4@SiO_2@MPS and Co(II)-MIIP.

3.9. Effect of Solution pH

Solution pH has a decisive effect on the existence of ions and the degree of protonation of the adsorbent and has an important position in the process of ion enrichment by the adsorbent. As shown in Figure 10a [25], Co(II) has four existing forms, namely Co^{2+}, $Co(OH)^+$, $Co(OH)_2$, and $Co(OH)_3^-$, in the pH range of 4.0 to 13.0. When pH < 8.0, the main existing form of Co(II) is Co^{2+}. Figure 10b showed the adsorption capacity of Co(II)-MIIP and Co(II)-NIP in the pH range of 3.0 to 8.5. Under acidic or neutral conditions (pH $\leq$ 7.0),

Co(II)-MIIP and Co(II)-NIP both exhibited poor adsorption capacity to Co(II) ions. Because the electrostatic repulsion between the protonated functional groups and the positively-charged Co(II) ions weakened the coordination interaction between the imprinted sites and Co(II) ions, resulting in the lower adsorption capacity [11]. When the pH of the solution was between 7.0 and 8.0, the adsorption capacity of both adsorbents increased with the increase of solution pH. At this time, the protonation of the functional groups on Co(II)-MIIP decreased, and the unprotonated functional groups could coordinate with Co(II) ions. Meanwhile, the electrostatic attraction between functional groups and Co(II) ions also contributed to the increase of adsorption capacity [39]. In addition, due to the imprinting effect of template ions, the adsorption capacity of Co(II)-MIIP for Co(II) ions was much higher than that of Co(II)-NIP. When the solution pH exceeded 8.0, high concentrations of Co(II) ions were easily precipitated [39]. Therefore, pH = 8 was the optimum pH value for subsequent adsorption experiments, which is consistent with previous studies [9,25].

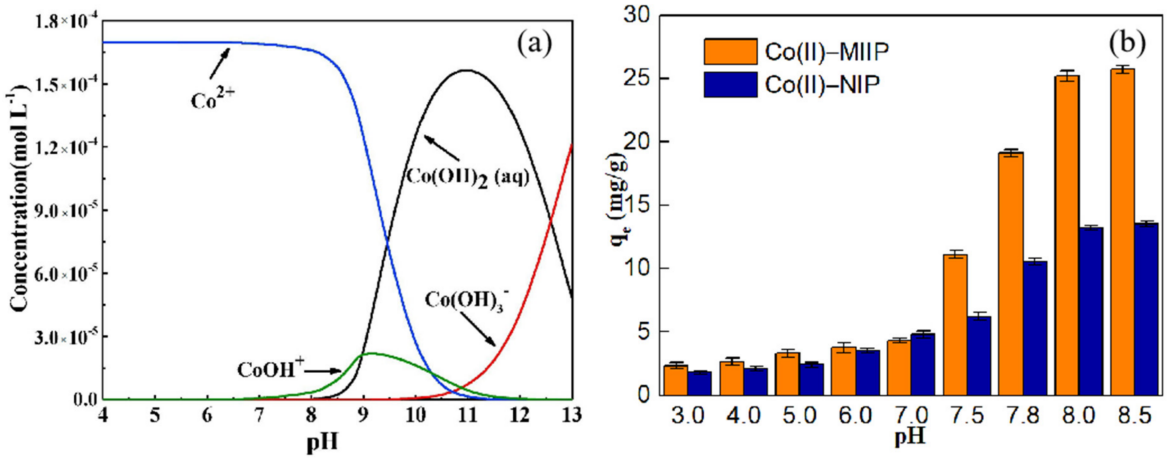

Figure 10. (**a**) Main species of Co(II) at different pH values (c = 10 mg·L^{-1}), (**b**) effect of pH on Co(II) adsorption onto Co(II)-MIIP and Co(II)-NIP, respectively.

3.10. Adsorption Kinetics

The kinetics of the adsorption process can provide relevant information about solute adsorption rate and adsorption model. The adsorption capacity of Co(II)-MIIP and Co (II)-NIP to Co(II) ions varied with adsorption duration, as shown in Figure 11a. Within the first five minutes, the adsorption capacity of Co(II)-MIIP increased rapidly, and nearly 85% of the total adsorption capacity occurred in this stage. After 20 min, adsorption equilibrium was achieved. For comparison, the adsorption rate of Co(II)-NIP was relatively uniform and slow. The adsorption equilibrium was reached after 30 min, which was longer than that of Co(II)–MIIP. Due to the lack of Co(II) ions template effect in Co(II)-NIP, the surface adsorption sites were less than that of Co(II)-MIIP, and the specific recognition between adsorbent and Co(II) ions was lacking. By comprehensive comparison, it could be seen that Co(II)–MIIP had the advantage of faster adsorption than Co(II)-NIP.

Pseudo-first-order (Equation (5)) and pseudo-second-order (Equation (6)) were used to fit the -experimental data, respectively [40,41].

$$q_t = q_e(1 - e^{-k_1 t}) \tag{5}$$

$$q_t = \frac{k_2 q_e^2}{1 + k_2 q_e t} t \tag{6}$$

where k_1 (min^{-1}) and k_2 (g·mg^{-1}·min^{-1}) are the pseudo-first-order and pseudo-second-order kinetic rate constants, respectively; q_t (mg·g^{-1}) and q_e (mg·g^{-1}) are the adsorption amount of Co(II) ions at time t and equilibrium, respectively.

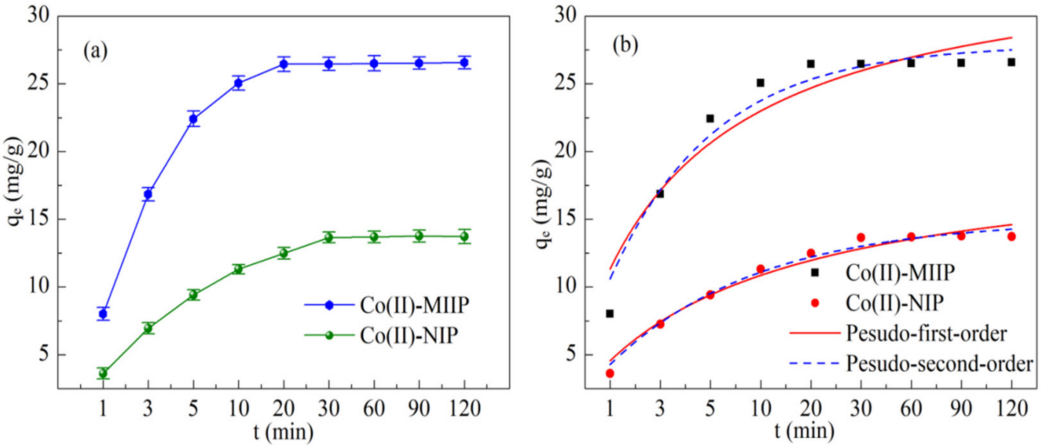

Figure 11. (**a**) Adsorption capacity changed over time; (**b**) fitting of Co(II) adsorption by Co(II)-MIIP and Co(II)-NIP to Co(II) (c = 100 mg·L^{-1}, 25 °C).

The kinetics models for the adsorption of Co(II) ions onto Co(II)-MIIP and Co(II)-NIP are shown in Figure 11b, and the relevant kinetics fitting parameters are listed in Table 2. Comparing R^2 of the pseudo-first-order and the pseudo-second-order fittings, it can be seen that the pseudo-second-order kinetics is more suitable to describe the adsorption process of Co(II) ions, which indicated that adsorption proceeded via chemical adsorption [42]. At the same time, it could be seen that the fitting degree of Co(II)-MIIP was closer to the experiment, which proved that Co(II)-MIIP had better performance than Co(II)-NIP.

Table 2. Fitting parameters of kinetic models for Co(II) adsorption by using Co(II)-MIIP and Co(II)-NIP.

	$q_{e,\ experimemt}$ (mg·g^{-1})	Pseudo-First-Order			Pseudo-Second-Order			
		k_1 (1·min^{-1})	q_e (mg·g^{-1})	R^2	k_2 (g·mg^{-1}·min^{-1})	q_e (mg·g^{-1})	h_0	R^2
Co(II)-MIIP	26.53	0.0119	35.43	0.906	0.433	27.85	1.78	0.955
Co(II)-NIP	13.72	0.0142	20.39	0.969	0.332	15.03	1.17	0.986

3.11. Adsorption Isotherm

The equilibrium adsorption isotherms were carried out with the original concentration ranges from 20–500 mg·L^{-1}, as shown in Figure 12. Adsorption capacity of Co(II)-MIIP and Co(II)-NIP increased rapidly with initial concentration of Co(II) ions increased from 20 to 100 mg·L^{-1}. The adsorption capacity increased gradually from 100 to 300 mg·L^{-1} and reached saturation when the concentration increased to 300 mg·L^{-1}. At this time, the active imprinted sites that can bind to Co(II) ions on the imprinted materials were all occupied [43], and the saturated adsorption capacities were 33.4 mg·g^{-1} and 15.7 mg·g^{-1}, respectively. The adsorption capacity of Co(II)-MIIP was far greater than that of Co(II)-NIP because several imprinted sites were emerged in the surface ion imprinting process.

Langmuir isotherm equation (Equation (7)) and Freundlich isotherm equation (Equation (8)) were used to fit the equilibrium adsorption experimental data, respectively [44,45].

$$\frac{C_e}{q_e} = \frac{C_e}{q_m} + \frac{1}{K_L q_m} \tag{7}$$

$$\ln q_e = \ln K_F + \frac{1}{n} \ln C_e \tag{8}$$

where C_e (mg·L^{-1}) is the Co(II) ion concentration in solution at adsorption equilibrium; q_e (mg·g^{-1}) is the adsorption capacity of Co(II) ions by adsorbents at adsorption equilibrium;

q_m (mg·g^{-1}) is the theoretical maximum adsorption capacity; K_L (L·mg^{-1}) is the Langmuir isotherm model constant; K_F (mg·g^{-1}) is the Freundlich isotherm model constant; and n represents the Freundlich isotherm model binding constant.

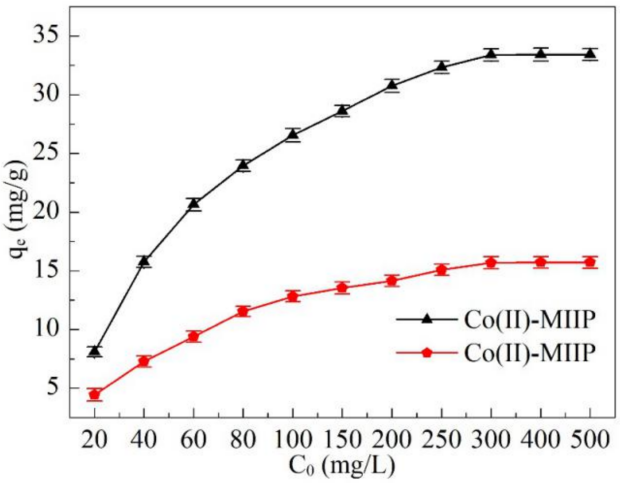

Figure 12. Effect of initial concentration of Co(II) on the adsorption capacity of Co(II)-MIIP and Co(II)-NIP.

The fitting curves are shown in Figure 13a,b, and the relevant fitting parameters are listed in Table 3. According to the data, the correlation coefficients (R^2) of the Langmuir model for Co(II)-MIIP and Co(II)-NIP were 0.995 and 0.997, respectively, while the R^2 of the Freundlich isotherm model were 0.839 and 0.865, respectively. It can be concluded that Langmuir isotherm model is more suitable to describe the adsorption process of Co(II)-MIIP and Co(II)-NIP, demonstrating that the adsorption of Co(II) ions by Co(II)-MIIP and Co(II)-NIP is a monolayer chemical adsorption, which is consistent with the conclusion of adsorption kinetics [46]. In addition, the theoretical maximum adsorption capacity of Co(II)-MIIP and Co(II)-NIP calculated by the Langmuir isotherm equation were 37.81 mg·g^{-1} and 17.54 mg·g^{-1}, respectively, which were closer to the experimental maximum adsorption capacities (33.43 mg·g^{-1} and 15.71 mg·g^{-1}). It also suggested that that Langmuir isotherm model was more suitable to describe the adsorption process of Co(II)-MIIP and Co(II)-NIP.

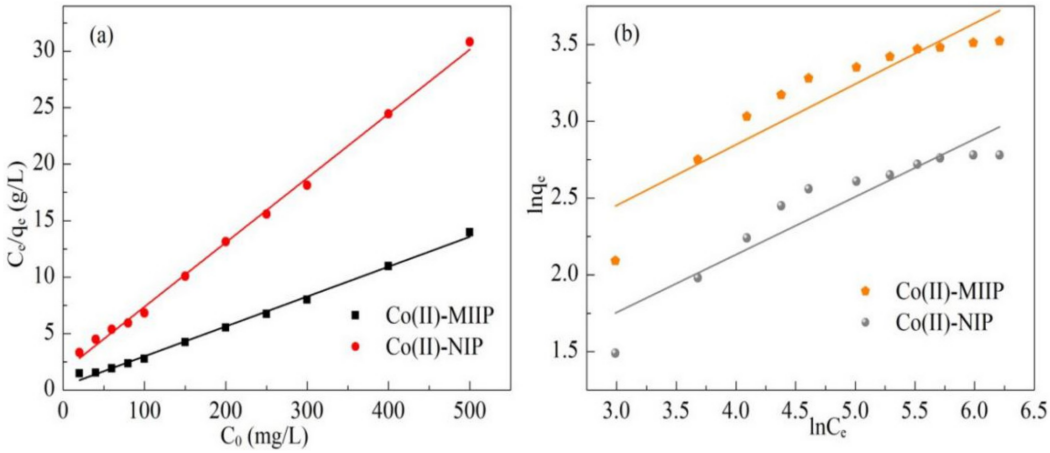

Figure 13. (**a**) Langmuir and (**b**) Freundlich fittings of Co(II) adsorption onto Co(II)-MIIP and Co(II)-NIP.

Table 3. Langmuir and Freundlich isotherm model parameters for Co(II) adsorption onto Co(II)-MIIP and Co(II)-NIP.

Adsorbents	Langmuir			Freundlich		
	$q_{m,\,experiment}$ (mg·g^{-1})	K_L (L·mg^{-1})	R^2	n	K_F (mg·g^{-1})	R^2
Co(II)-MIIP	37.81	0.076	0.995	1.26	14.93	0.839
Co(II)-NIP	17.54	0.034	0.997	1.59	12.68	0.865

3.12. Adsorption Selectivity

Binary competitive system

In this experiment, Cu(II), Zn(II), Ni(II), Mg(II), and Fe(II) ions, which possessed the same valence state and similar ion radius as Co(II) ions, were selected as competitive ions to explore the adsorption selectivity of Co(II)-MIIP and Co(II)-NIP. The adsorption capacities of Co(II)-MIIP and Co(II)-NIP for Co(II) ions and various competitive ions are illustrated in Table 4. The distribution coefficient (K_d, L·g^{-1}), selection coefficient (K), and relative selectivity coefficient (K') calculated by Equations (2)–(4) are listed in Table 4. Co(II)-MIIP had adsorption effect on all ions in the solution, indicating that Co(II)-MIIP had an enrichment effect on template ions and ions with similar structure, but the adsorption capacity of competitive ions was significantly lower than that of Co(II) ions, indicating that Co(II)-MIIP had strong selective recognition on template ions [27]. In contrast, the adsorption capacity of Co(II)-NIP for competitive ions was not significantly different from that of Co(II) ions, because the lack of template ions led to fewer adsorption sites and irregular three-dimensional structure in the preparation of Co(II)–NIP. In addition, in the presence of different competitive ions, the K' parameter was greater than 1, which also showed that the selective recognition of Co(II)-MIIP was better than Co(II)-NIP [27,40].

Table 4. Distribution coefficient, selectivity coefficient, and relative selectivity coefficient for Co(II)-MIIP and Co(II)-NIP.

Ions	Co(II)-MIIP			Co(II)-NIP			K'
	q (mg·g^{-1})	K_d	K	q (mg·g^{-1})	K_d	K	
Co(II)	20.8	0.263	6.41	7.7	0.083	1.22	5.25
Fe(II)	3.9	0.041	-	6.4	0.068	-	-
Co(II)	22.4	0.29	5.15	9.2	0.101	1.27	4.05
Cu(II)	5.3	0.056	-	7.4	0.08	-	-
Co(II)	21.6	0.285	7.37	8.4	0.092	1.21	6.09
Mg(II)	3.7	0.038	-	7.1	0.076	-	-
Co(II)	24.5	0.263	10.42	7.3	0.079	0.87	11.82
Zn(II)	2.4	0.025	-	8.2	0.088	-	-
Co(II)	19.3	0.248	3.64	6.5	0.069	0.81	4.48
Ni(II)	6.2	0.066	-	7.8	0.085	-	-

Multicomponent competitive system

There are many kinds of ions in industrial wastewater, so it is necessary to investigate the adsorption selectivity of Co(II)-MIIP and Co(II)-NIP for Co(II) in a multicomponent competitive system, which may contain Co(II), Cu(II), Zn(II), Ni(II), Mg(II), and Fe(II) ions in the solution. The competitive ions used in binary competitive system were also selected to simulate a multicomponent competitive system and investigate the adsorption selectivity of prepared adsorbents, with concentration of 100 mg·L^{-1} each. As shown in Figure 14, compared with the binary competitive system, both the adsorption capacity of Co(II)-MIIP and Co(II)-NIP for Co(II) ions reduced. However, the adsorption capacity of Co(II)-MIIP for Co(II) ions was still at least three times that of competitive ions, and there was still no significant difference in the adsorption capacity of Co(II)-NIP for Co(II) ions and competitive ions because of the poor selectivity of Co(II)-NIP. The results showed that

Co(II)-MIIP exhibited good adsorption selectivity for template ions even in the presence of various competitive ions.

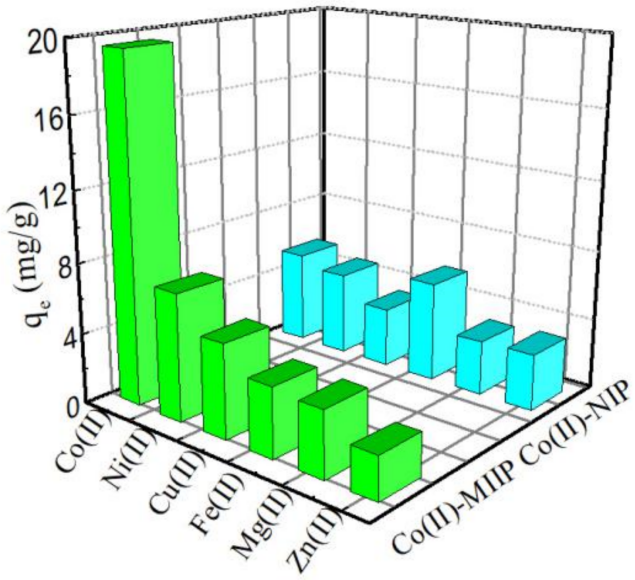

Figure 14. Adsorption capacity of different competitive ions onto Co(II)-MIIP and Co(II)-NIP.

3.13. Reusability

Reusability of adsorbents is one of the important means to save treatment costs. In addition to excellent selectivity, better recycling performance is another advantage of imprinted materials. Six adsorption–desorption cycles were performed to study the reusability of magnetic Co(II)-MIIP, and 0.05 mol·L^{-1} NaOH solution was used as the eluent. As given in Figure 15, the adsorption capacity of Co(II)-MIIP decreased from 26.30 mg·g^{-1} to 23.40 mg·g^{-1} after six adsorption–desorption cycles, retaining 89% of its initial adsorption capability. Experimental results demonstrate that there was no serious damage to the imprinting recognition sites of the adsorbent after repeated adsorption and elution [47]. Therefore, the prepared Co(II)-MIIP has excellent stability and reusability. The comparison of Co(II)-MIIP with other adsorbents reported was listed in Table 5.

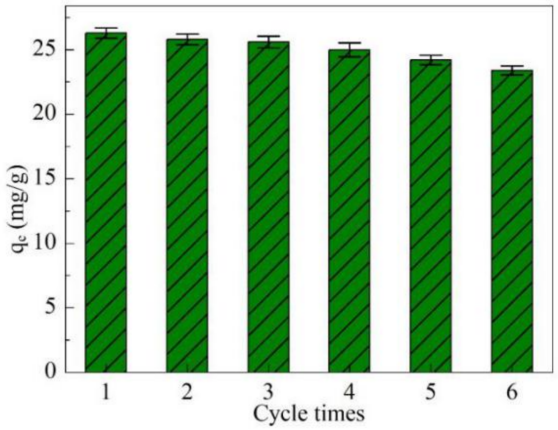

Figure 15. Reusability of Co(II)-MIIP for Co(II) removal.

Table 5. Comparison of adsorption performances of different adsorbents for Co(II).

Adsorbents	Capacity ($mg \cdot g^{-1}$)	Equilibrium Time (min)	Cycles	Selectivity	Ref.
DCPD	441	1440	-	No	[9]
IIP-MAA	15.38	20	5	Poor	[12]
UiO-66-NH_2	175.0	1200	5	Yes	[25]
P-IIPs	96.65	60	3	Yes	[2]
IIPMO	109.6098	30	5	Yes	[48]
Slag-Ox	576	120	3	No	[49]
Co(II)-MIIP	33.4	20	6	Yes	This study

We have compared the adsorbent with previously reported adsorbents regarding adsorption capacity, time, reusability, and adsorption selectivity, and the results are listed in Table 5. It can be concluded from the table that the equilibrium time and the reused cycles of the prepared Co(II)-MIIP were better or comparable in respect to other reports. Meanwhile, it showed excellent selectivity.

4. Conclusions

A novel ion-imprinted polymer Co(II)-MIIP with magnetic property was synthesized for the rapidly and efficiently selective separation of Co(II) from aqueous solution. Through the analysis of various characterizations about its morphology and structure, Co(II)-MIIP was a kind of mesoporous adsorbent with high stability that can be used for ion adsorption. It achieved better filtration and recovery by applying an external magnetic field. The combination of dual monomers (B-2MP and GG with molar ratio of 4:1) and surface ion imprinting technology then gives it a better selectivity. In the binary competition system and the multiple competition system, it showed that Co(II)-MIIP had good adsorption selectivity and strong anti-interference ability. At the same time, it also had a stable reusability; the adsorption capacity dropped only 11% after six consecutive adsorption–elution cycles so as to realize the fast and efficient adsorption of Co(II) from the aqueous solution containing various ions.

Author Contributions: Conceptualization, Z.L. and W.G.; formal analysis, Z.Z. and L.W.; methodology, H.J., N.Y., and L.W.; writing—original draft preparation, Z.Z., H.J., and L.W.; writing—review and editing, Z.L. and W.G. All authors have read and agreed to the published version of the manuscript.

Funding: This research was funded by the National Natural Science Foundation of China (grant number 22078157), the Natural Science Foundation of the Jiangsu Higher Education institutions of China (grant number 21KJB610011) and Postgraduate Research and Practice Innovation Program of Jiangsu Province (grant number SJCX21_0468).

Conflicts of Interest: The authors declare no conflict of interest.

References

1. Dehaine, Q.; Tijsseling, L.T.; Glass, H.J.; Törmänen, T.; Butcher, A.R. Geometallurgy of cobalt ores: A review. *Miner. Eng.* **2021**, *160*, 106656. [CrossRef]
2. Liu, Y.; Zhong, G.; Liu, Z.; Meng, M.; Jiang, Y.; Ni, L.; Guo, W.; Liu, F. Preparation of core-shell ion imprinted nanoparticles via photoinitiated polymerization at ambient temperature for dynamic removal of cobalt in aqueous solution. *RSC Adv.* **2015**, *5*, 85691–85704. [CrossRef]
3. Khoddami, N.; Shemirani, F. A new magnetic ion-imprinted polymer as a highly selective sorbent for determination of cobalt in biological and environmental samples. *Talanta* **2016**, *146*, 244–252. [CrossRef]
4. Torkashvand, M.; Gholivand, M.B.; Azizi, R. Synthesis, characterization and application of a novel ion-imprinted polymer based voltammetric sensor for selective extraction and trace determination of cobalt (II) ions. *Sens. Actuat. B-Chem.* **2017**, *243*, 283–291. [CrossRef]
5. Biswal, B.K.; Jadhav, U.U.; Madhaiyan, M.; Ji, L.; Yang, E.; Cao, B. Biological leaching and chemical precipitation methods for recovery of Co and Li from spent lithium-ion batteries. *ACS Sustain. Chem. Eng.* **2018**, *6*, 12343–12352. [CrossRef]

6. Ren, J.; Li, R.; Liu, Y.; Cheng, Y.; Mu, D.; Zheng, R.; Liu, J.; Dai, C. The impact of aluminum impurity on the regenerated lithium nickel cobalt manganese oxide cathode materials from spent LIBs. *New J. Chem.* **2017**, *41*, 10959–10965. [CrossRef]
7. Alkhadra, M.A.; Conforti, K.M.; Gao, T.; Tian, H.; Bazant, M.Z. Continuous separation of radionuclides from contaminated water by shock electrodialysis. *Environ. Sci. Technol.* **2020**, *54*, 527–536. [CrossRef]
8. Tortora, F.; Innocenzi, V.; De Michelis, I.; Vegliò, F.; di Celso, G.M.; Prisciandaro, M. Recovery of anionic surfactant through acidification/ultrafiltration in a micellar-enhanced ultrafiltration process for Cobalt removal. *Environ. Eng. Sci.* **2018**, *35*, 493–500. [CrossRef]
9. Vivas, E.L.; Cho, K. Efficient adsorptive removal of Cobalt(II) ions from water by dicalcium phosphate dihydrate. *J. Environ. Manag.* **2021**, *283*, 111990. [CrossRef]
10. Saleh, T.A.; Musa, A.M.; Tawabini, B.; Ali, S.A. Aminomethylphosphonate chelating ligand and octadecyl alkyl chain in a resin for simultaneous removal of Co(II) ions and organic contaminants. *J. Chem. Eng. Data* **2016**, *61*, 3377–3385. [CrossRef]
11. Hossein Beyki, M.; Shemirani, F.; Shirkhodaie, M. Aqueous Co(II) adsorption using 8-hydroxyquinoline anchored γ-Fe_2O_3@chitosan with Co(II) as imprinted ions. *Int. J. Biol. Macromol.* **2016**, *87*, 375–384. [CrossRef] [PubMed]
12. Yusof, N.F.; Mehamod, F.S.; Mohd Suah, F.B. Fabrication and binding characterization of ion imprinted polymers for highly selective Co^{2+} ions in an aqueous medium. *J. Environ. Chem. Eng.* **2019**, *7*, 103007. [CrossRef]
13. Şarkaya, K.; Demir, A. The comparative investigation on synthesis, characterizations of silver ion-imprinting and non-imprinting cryogels, their impedance spectroscopies and relaxation mechanisms. *Polym. Bull.* **2019**, *76*, 5701–5716. [CrossRef]
14. Chaipuang, A.; Phungpanya, C.; Thongpoon, C.; Watla-Iad, K.; Inkaew, P.; Machan, T.; Suwantong, O. Synthesis of copper(II) ion-imprinted polymers via suspension polymerization. *Polym. Adv. Technol.* **2018**, *29*, 3134–3141. [CrossRef]
15. Huang, R.; Ma, X.; Li, X.; Guo, L.; Xie, X.; Zhang, M.; Li, J. A novel ion-imprinted polymer based on graphene oxide-mesoporous silica nanosheet for fast and efficient removal of chromium (VI) from aqueous solution. *J. Colloid Interf. Sci.* **2018**, *514*, 544–553. [CrossRef] [PubMed]
16. Zhang, L.; Xue, J.; Zhou, X.; Fei, X.; Wang, Y.; Zhou, Y.; Zhong, L.; Han, X. Adsorption of molybdate on molybdate-imprinted chitosan/triethanolamine gel beads. *Carbohyd. Polym.* **2014**, *114*, 514–520. [CrossRef]
17. Lee, H.; Choi, J.; Choi, S. Magnetic ion-imprinted polymer based on mesoporous silica for selective removal of Co(II) from radioactive wastewater. *Sep. Sci. Technol.* **2021**, *56*, 1842–1852. [CrossRef]
18. Wang, R.; Lin, J.; Huang, S.; Wang, Q.; Hu, Q.; Peng, S.; Wu, L.; Zhou, Q. Disulfide cross-linked poly(methacrylic acid) iron oxide nanoparticles for efficiently selective adsorption of Pb(II) from aqueous solutions. *ACS Omega* **2021**, *6*, 976–987. [CrossRef]
19. Dahaghin, Z.; Mousavi, H.Z.; Boutorabi, L. Application of magnetic ion-imprinted polymer as a new environmentally-friendly nonocomposite for a selective adsorption of the trace level of Cu(II) from aqueous solution and different samples. *J. Mol. Liq.* **2017**, *243*, 380–386. [CrossRef]
20. Wu, L.; Luo, Z.; Jiang, H.; Zhao, Z.; Geng, W. Selective and rapid removal of Mo(VI) from water using functionalized Fe_3O_4-based Mo(VI) ion-imprinted polymer. *Water Sci. Technol.* **2021**, *83*, 435–448. [CrossRef]
21. Qian, J.; Zhang, S.; Zhou, Y.; Dong, P.; Hua, D. Synthesis of surface ion-imprinted magnetic microspheres by locating polymerization for rapid and selective separation of uranium (VI). *RSC Adv.* **2015**, *5*, 4153–4161. [CrossRef]
22. Zhao, B.; He, M.; Chen, B.; Hu, B. Fe_3O_4 nanoparticles coated with double imprinted polymers for magnetic solid phase extraction of lead(II) from biological and environmental samples. *Microchim. Acta* **2019**, *186*, 1–11. [CrossRef] [PubMed]
23. Luo, X.; Liu, L.; Deng, F.; Luo, S. Novel ion-imprinted polymer using crown ether as a functional monomer for selective removal of Pb(II) ions in real environmental water samples. *J. Mater. Chem. A* **2013**, *1*, 8280–8286. [CrossRef]
24. Wang, H.; Shang, H.; Sun, X.; Hou, L.; Wen, M.; Qiao, Y. Preparation of thermo-sensitive surface ion-imprinted polymers based on multi-walled carbon nanotube composites for selective adsorption of lead(II) ion. *Colloid Surface A* **2020**, *585*, 124139. [CrossRef]
25. Yuan, G.; Tu, H.; Liu, J.; Zhao, C.; Liao, J.; Yang, Y.; Yang, J.; Liu, N. A novel ion-imprinted polymer induced by the glycylglycine modified metal-organic framework for the selective removal of Co(II) from aqueous solutions. *Chem. Eng. J.* **2018**, *333*, 280–288. [CrossRef]
26. Kong, D.; Wang, N.; Qiao, N.; Wang, Q.; Wang, Z.; Zhou, Z.; Ren, Z. Facile preparation of ion-imprinted chitosan microspheres enwrapping Fe_3O_4 and graphene oxide by inverse suspension cross-linking for highly selective removal of copper(II). *ACS Sustain. Chem. Eng.* **2017**, *5*, 7401–7409. [CrossRef]
27. Xie, C.; Huang, X.; Wei, S.; Xiao, C.; Cao, J.; Wang, Z. Novel dual-template magnetic ion imprinted polymer for separation and analysis of Cd^{2+} and Pb^{2+} in soil and food. *J. Clean. Prod.* **2020**, *262*, 121387. [CrossRef]
28. Zhou, Z.; Liu, X.; Zhang, M.; Jiao, J.; Zhang, H.; Du, J.; Zhang, B.; Ren, Z. Preparation of highly efficient ion-imprinted polymers with Fe_3O_4 nanoparticles as carrier for removal of Cr(VI) from aqueous solution. *Sci. Total Environ.* **2020**, *699*, 134334. [CrossRef]
29. Guo, H.; Tang, Y.; Yu, Y.; Xue, L.; Qian, J. Covalent immobilization of α-amylase on magnetic particles as catalyst for hydrolysis of high-amylose starch. *Int. J. Biol. Macromol.* **2016**, *87*, 537–544. [CrossRef] [PubMed]
30. Liu, G.; Wang, H.; Yang, X.; Li, L. Synthesis of tri-layer hybrid microspheres with magnetic core and functional polymer shell. *Eur. Polym. J.* **2009**, *45*, 2023–2032. [CrossRef]
31. Zhu, G.; Tang, H.; Qing, P.; Zhang, H.; Cheng, X.; Cai, Z.; Xu, H.; Zhang, Y. A monophosphonic group-functionalized ion-imprinted polymer for a removal of Fe^{3+} from highly concentrated basic chromium sulfate solution. *Korean J. Chem. Eng.* **2020**, *37*, 911–920. [CrossRef]

32. Al-Ghouti, M.A.; Dib, S.S. Utilization of nano-olive stones in environmental remediation of methylene blue from water. *J. Environ. Health Sci.* **2020**, *18*, 63–77. [CrossRef] [PubMed]
33. Lu, B.; Zhu, Y.; Ao, H.; Qi, C.; Chen, F. Synthesis and characterization of magnetic iron oxide/calcium silicate mesoporous nanocomposites as a promising vehicle for drug delivery. *ACS Appl. Mater. Inter.* **2012**, *4*, 6969–6974. [CrossRef]
34. Akbarnejad, S.; Amooey, A.A.; Ghasemi, S. High effective adsorption of acid fuchsin dye using magnetic biodegradable polymer-based nanocomposite from aqueous solutions. *Microchem. J.* **2019**, *149*, 103966. [CrossRef]
35. Hassan, S.H.; Kamel, A.; Hassan, A.A.; Amr, A.; Abd El-Naby, H.; Al-Omar, M.; Sayed, A. $CuFe_2O_4$/polyaniline (PANI) nanocomposite for the hazard mercuric ion removal: Synthesis, characterization, and adsorption properties study. *Molecules* **2020**, *25*, 2721. [CrossRef]
36. Tan, P.; Jiang, Y.; Liu, X.; Sun, L. Magnetically responsive porous materials for efficient adsorption and desorption processes. *Chin. J. Chem. Eng.* **2019**, *27*, 1324–1338. [CrossRef]
37. Fayazi, M.; Taher, M.A.; Afzali, D.; Mostafavi, A.; Ghanei-Motlagh, M. Synthesis and application of novel ion-imprinted polymer coated magnetic multi-walled carbon nanotubes for selective solid phase extraction of lead(II) ions. *Mater. Sci. Eng. C* **2016**, *60*, 365–373. [CrossRef]
38. Shafizadeh, F.; Taghizadeh, M.; Hassanpour, S. Preparation of a novel magnetic Pd(II) ion-imprinted polymer for the fast and selective adsorption of palladium ions from aqueous solutions. *Environ. Sci. Pollut. R* **2019**, *26*, 18493–18508. [CrossRef] [PubMed]
39. Adibmehr, Z.; Faghihian, H. Preparation of highly selective magnetic cobalt ion-imprinted polymer based on functionalized SBA-15 for removal Co^{2+} from aqueous solutions. *J. Environ. Health Sci.* **2019**, *17*, 1213–1225. [CrossRef]
40. Wang, L.; Li, J.; Wang, J.; Guo, X.; Wang, X.; Choo, J.; Chen, L. Green multi-functional monomer based ion imprinted polymers for selective removal of copper ions from aqueous solution. *J. Colloid Interf. Sci.* **2019**, *541*, 376–386. [CrossRef]
41. Velempini, T.; Pillay, K.; Mbianda, X.Y.; Arotiba, O.A. Carboxymethyl cellulose thiol-imprinted polymers: Synthesis, characterization and selective Hg(II) adsorption. *J. Environ. Sci. China* **2019**, *79*, 280–296. [CrossRef] [PubMed]
42. Moussa, S.I.; Ali, M.M.S.; Sheha, R.R. The performance of activated carbon/$NiFe_2O_4$ magnetic composite to retain heavy metal ions from aqueous solution. *Chin. J. Chem. Eng.* **2021**, *29*, 135–145. [CrossRef]
43. Neolaka, Y.A.B.; Lawa, Y.; Naat, J.N.; Pau Riwu, A.A.; Darmokoesoemo, H.; Supriyanto, G.; Holdsworth, C.I.; Amenaghawon, A.N.; Kusuma, H.S. A Cr(VI)-imprinted-poly(4-VP-co-EGDMA) sorbent prepared using precipitation polymerization and its application for selective adsorptive removal and solid phase extraction of Cr(VI) ions from electroplating industrial wastewater. *Reat. Funct. Polym.* **2020**, *147*, 104451. [CrossRef]
44. Li, M.; Feng, J.; Huang, K.; Tang, S.; Liu, R.; Li, H.; Ma, F.; Meng, X. Amino group functionalized SiO_2@graphene oxide for efficient removal of Cu(II) from aqueous solutions. *Chem. Eng. Res. Des.* **2019**, *145*, 235–244. [CrossRef]
45. Kenawy, I.M.; Ismail, M.A.; Hafez, M.A.H.; Hashem, M.A. Synthesis and characterization of novel ion-imprinted guanyl-modified cellulose for selective extraction of copper ions from geological and municipality sample. *Int. J. Biol. Macromol.* **2018**, *115*, 625–634. [CrossRef] [PubMed]
46. Al Abri, A.M.; Mohamad, S.; Abdul Halim, S.N.; Abu Bakar, N.K. Development of magnetic porous coordination polymer adsorbent for the removal and preconcentration of Pb(II) from environmental water samples. *Environ. Sci. Pollut. R* **2019**, *26*, 11410–11426. [CrossRef]
47. Nchoe, O.B.; Klink, M.J.; Mtunzi, F.M.; Pakade, V.E. Synthesis, characterization, and application of β-cyclodextrin-based ion-imprinted polymer for selective sequestration of Cr(VI) ions from aqueous media: Kinetics and isotherm studies. *J. Mol. Liq.* **2020**, *298*, 111991. [CrossRef]
48. Moorthy, M.S.; Tapaswi, P.K.; Park, S.S.; Mathew, A.; Cho, H.; Ha, C. Ion-imprinted mesoporous silica hybrids for selective recognition of target metal ions. *Micropor. Mesopor. Mat.* **2013**, *180*, 162–171. [CrossRef]
49. Le, Q.T.N.; Vivas, E.L.; Cho, K. Oxalated blast-furnace slag for the removal of Cobalt(II) ions from aqueous solutions. *J. Ind. Eng. Chem.* **2021**, *95*, 57–65. [CrossRef]